Die Pharmazie

Pharmazie **2026**; 81(7): 52723
https://doi.org/10.31083/Pharmazie52723

Research Article

SCM198 Alleviates Pulmonary Fibrosis Through Downregulation of the TGF-β1/Smad Signalling Pathway and Activation of Nrf2-Mediated Antioxidant Defenses During EMT

Jie Liang[1,2,*], Hanxuan Wang[1,2], Ruixiang Wang[1,2], Keyuan Chen[2,3], Yizhun Zhu[2,3,4]

[1]Faculty of Chinese Medicine, Macau University of Science and Technology, 999078 Macau, China
[2]State Key Laboratory of Mechanism and Quality of Chinese Medicine, Macau University of Science and Technology, 999078 Macau, China
[3]School of Pharmacy, Macau University of Science and Technology, 999078 Macau, China
[4]Shanghai Key Laboratory of Bioactive Small Molecules and Department of Pharmacology, School of Pharmacy, Fudan University, 200000 Shanghai, China
*Correspondence: jliang@must.edu.mo (Jie Liang)
Academic Editors: Daniel J. V. A. dos Santos and Walter E. Müller
Submitted: 8 April 2026 Revised: 2 June 2026 Accepted: 18 June 2026 Published: 22 July 2026

Abstract

Background: Pulmonary fibrosis (PF) is a chronic and progressive respiratory disorder marked by aberrant activation of pulmonary fibroblasts and the occurrence of epithelial–mesenchymal transition (EMT) in alveolar epithelial cells (AECs). This disease process is primarily driven by inflammation and oxidative stress (OS), leading to excessive deposition of the extracellular matrix (ECM). Current treatments provide limited efficacy and are associated with significant side effects. Leonurine and its sulfate derivative SCM198, derived from Herba Leonuri, exhibit anti-inflammatory and antioxidant properties. However, their therapeutic effects and mechanisms of action in PF remain poorly understood. **Methods:** Bleomycin (BLM) was delivered intratracheally to mice to establish a model of PF. Human Fetal Lung fibroblast-1 (HFL-1) fibroblasts and A549 AECs were subjected to transforming growth factor-beta 1 (TGF-β1) exposure for *in vitro* assays. This study comprehensively evaluated the effects of SCM198 on PF and explored its underlying molecular mechanisms through metabolomics analysis, western blotting, and additional biological techniques. **Results:** SCM198 significantly ameliorated lung pathology and micro-Computed Tomography (CT) findings and reduced collagen deposition in BLM-treated mice. Furthermore, the levels of inflammatory markers and cytokines were decreased in lung tissue and Bronchoalveolar Lavage Fluid (BALF). *In vitro*, SCM198 inhibited fibroblast activation, EMT, and OS. It also down-regulated the TGF-β1/Smad2/3 pathway and activated the nuclear factor erythroid 2-related factor 2 (Nrf2) antioxidant pathway. **Conclusions:** The ameliorative action of SCM198 on BLM-induced pulmonary fibrosis is associated with suppression of the TGF-β1/Smad2/3 signaling axis and activation of Nrf2-mediated antioxidant defenses during the EMT process. However, further studies are needed to confirm the direct involvement of these pathways.

Keywords: pulmonary fibrosis (PF); SCM198; epithelial-mesenchymal transition (EMT); oxidative stress (OS); Keap-1/Nrf2/HO-1; TGF-β1/Smad2/3

1. Introduction

Pulmonary fibrosis (PF) represents a debilitating pulmonary disorder distinguished by substantial extracellular matrix (ECM) accumulation and lung structural, remodeling, which progressively lead to respiratory dysfunction and potential mortality [1,2]. Its etiology is multifactorial, involving environmental exposure, autoimmune conditions, drug toxicity, radiation, and postviral sequelae, increasingly observed in COVID-19 survivors due to SARS-CoV-2-induced pulmonary damage [3,4]. There remains no consensus on the pathogenesis of PF. Central to the pathogenesis and progression of PF are lung fibroblast activation and alveolar epithelial–mesenchymal transition (EMT) [5]. Following lung injury, an overproduction of reactive oxygen species (ROS) induces oxidative stress (OS) and triggers pulmonary inflammatory responses. This inflammatory cascade, marked by an excess of ROS, serves as a key initiator of pulmonary inflammation. OS and inflammation synergistically stimulate the synthesis and secretion of multiple cytokines, which subsequently drive alveolar epithelial cell (AEC) EMT, fibroblast activation, collagen synthesis, and ECM deposition, processes that collectively lead to the development of PF. Therefore, targeting OS may represent a promising therapeutic approach for PF [6].

Multiple cytokines and signaling pathways contribute to the pathogenesis and progression of PF. Among these factors, transforming growth factor-beta 1 (TGF-β1) acts as a central mediator. It stimulates both lung fibroblast activation and AEC EMT while driving the expression and pathological deposition of ECM proteins. Upon release, TGF-β1 activates the TGF-β1/Smad pathway. Accordingly, upregulating key profibrotic proteins, encompassing collagen, fibronectin, and α-smooth muscle actin (α-SMA), can be upregulated. Given the pivotal role of TGF-β1, pharmacological inhibition of the TGF-β1/Smad pathway has emerged as a promising therapeutic strategy for PF [7]. Nuclear fac-

tor erythroid 2-related factor 2 (Nrf2) is an essential regulator of cellular antioxidant responses. Under physiological conditions, Nrf2 is sequestered in the cytoplasm through its association with Kelch-like ECH-associated protein 1 (Keap1). In response to oxidative stress, Nrf2 dissociates from Keap1, translocates into the nucleus, and initiates the transcription of antioxidant enzymes such as heme oxygenase-1 (HO-1), thereby enhancing the cell's defense against oxidative damage [8,9]. Activation of the Nrf2 pathway has shown potential in inhibiting TGF-β/Smad-mediated profibrotic signaling.

SCM198 is the sulfate form of leonurine, an active ingredient extracted from the traditional Chinese medicine Leonurus japonicus. Previous investigations conducted by our research group have shown that SCM198 cells can resist rheumatoid arthritis, OS, and apoptosis in bone marrow mesenchymal stem cells [10,11,12,13]. The effects and molecular basis of SCM198 in pulmonary fibrosis have not been fully elucidated. PF was modeled in mice using BLM administration, and cell-based experiments involved TGF-β-treated Human Fetal Lung fibroblast-1 (HFL-1) fibroblasts and A549 epithelial cells.This approach enabled us to systematically evaluate the antifibrotic effects of SCM198 and elucidate its underlying molecular mechanisms.

2. Materials and Methods

2.1 Antibodies and Reagents

SCM198 was synthesized and purified by our group (>99% purity). TGF-β1 (0122209, Peprotech), BLM (3408421, Nippon Kayaku), and pirfenidone (PFD) (H20133376, Beijing Contini) were purchased from commercial sources. Antibodies against Nrf2 (1:500, 12721), HO-1 (1:1000, 82206), Keap-1 (1:1000, 8047), Interleukin-6 (IL-6, 1:1000, 12912), Tumor necrosis factor (TNF-α, 1:1000, 11948), p-Smad2 (1:1000, 3108), p-Smad3 (1:1000, 9520), Smad2/3 (1:1000, 8685), Alpha-Smooth Muscle Actin (α-SMA, 1:1000, 19245), Collagen Type I Alpha 1 Chain (COL1A1) (1:1000, 72026), Fibronectin (1:1000, 26836),Vimentin (1:1000, 5741), E-cadherin (1:1000, 3195), N-cadherin (1:1000, 13116), GAPDH (1:1000, 5174) and Secondary antibody (Anti-rabbit, 1:8000, 7074) were purchased from CST (Danvers, Massachusetts, USA). Detection kits for superoxide dismutase (SOD) (S0109), malondialdehyde (MDA) (S0131S), and glutathione (GSH) (S0057S) were purchased from Beyotime (Shanghai, China). TNF-α (SEKM-0034) and IL-6 (SEKM-0007) were purchased from Nanjing Jiancheng (Nanjing, China). The cell culture reagents (RPMI-1640/22409015, FBS/16140071, and double antibody/15140148) were obtained from Gibco (Waltham, Massachusetts, USA).

2.2 Animal Model Replication and Treatment

Male C57BL/6J mice were purchased from Zhuhai Bestest Bio-Tech Co., Ltd. (Licence No. SCXK-(yue)-2020-0051), and mice weighing 22–25 g and 8 weeks of age were used in this study. All animals were maintained under standard laboratory conditions, including a temperature of 20–26 °C, humidity of 40–70%, a 12-hour light/dark cycle, and free access to food and water. Animal study was conducted in strict accordance with the ethical guidelines of the ARRIVE guidelines. All animal procedures complied with institutional ethical standards and received approval from the Macau University of Science and Technology Ethics Committee (Approval No.: MUST-SSTIC-20250507001). Mice were randomly distributed into six groups: control, BLM (2.5 mg/kg), BLM+PFD (234 mg/kg), and BLM+SCM198 (50, 100, 200 mg/kg). The method for establishing the PF model has been described previously [14]. This study involved 28 days of oral gavage administration (with SCM198 or PFD) in a mouse model. After the 28-day experimental period, the mice were anesthetized via intraperitoneal injection of sodium pentobarbital at a dose of 40 mg/kg, using a 2% (w/v) sodium pentobarbital solution. Adequate depth of anesthesia was confirmed by the loss of righting reflex and lack of response to paw pinch. The mice were then euthanized by cervical dislocation. Following confirmation of the cessation of heartbeat and respiratory movements, tissue collection was performed.

2.3 Cell Culture

The HFL-1 and A549 cell lines were obtained from Procell (Cat. No. CL0106, CL-0016, Wuhan, China) and cells between passages 3 and 10 were used. Both cell lines were cultured in RPMI-1640 medium supplemented with 10% fetal bovine serum (FBS) and 1% Penicillin–Streptomycin (PS), and maintained in a 37 °C incubator with a 5% CO_2 atmosphere. Treatment involved administering TGF-β1 (10 ng/mL) or various concentrations of SCM198 (5, 10, or 20 μM) for 24 hours before the The cells were harvested for further analysis. Prior to use, all cell lines were tested for mycoplasma contamination using the Mycoplasma Detection Kit (M107841, Shanghai ML-BIO) and confirmed to be free of mycoplasma contamination. Additionally, the identity of all cell lines used in this study was verified shortly before use by short tandem repeat (STR) profiling performed in our laboratory to confirm their species origin and authentic genetic background. The Ethics Committee of Macau University of Science and Technology approved all study protocols (Approval No.: MUST-SSTIC-20250507001), and the study was carried out in accordance with the ARRIVE guidelines.

2.4 Detection of Bronchoalveolar Lavage Fluid (BALF)

BALF samples were spun at 3000 rpm for 10 minutes at 4 °C. The resulting supernatant was collected for protein quantification using the bicinchoninic acid (BCA) assay. Levels of TNF-α and IL-6 in the supernatant were measured with Enzyme-Linked Immunosorbent Assay (ELISA)

kits, following the manufacturer's protocol. The cell pellet was reconstituted, and total cell numbers along with counts of macrophages, eosinophils, and neutrophils were determined using a Luna automated cell counter (Logos Biosystems, Anyang-si, Gyeonggi-do, Korea).

2.5 HE Staining, Masson Staining and Immunohistochemistry of the Lung

Histological examination began with perfusion of physiological saline into the lung vasculature via the heart to wash out the blood. This step was followed by bronchial perfusion with 4% paraformaldehyde (PFA) to prevent alveolar collapse. The lungs were then fixed in 4% PFA, embedded in paraffin, sectioned, deparaffinized, and dehydrated. Hematoxylin and Eosin (H&E) staining was conducted to assess histopathological changes using the Ashcroft scale. Collagen deposition was quantified with ImageJ software (1.53t, National Institutes of Health (NIH), Bethesda, MD, USA). For the immunohistochemical analysis of Nrf2 sections were treated with primary antibody at 4 °C overnight and secondary antibody at room temperature (20 °C) for one hour, followed by mounting in neutral resin. Nrf2 expression was evaluated using an inverted microscope IX73 (Olympus Corporation, Tokyo, Japan).

2.6 Micro-CT

PF mice, anesthetized with sodium pentobarbital, underwent micro-Computed Tomography (CT) imaging using a SKYSCAN 1176 system (Bruker Corporation, Kontich, Belgium). The chosen parameters were 65 kV, 298 μA, with a resolution of 2000 × 2000, using a 1.0 mm Al filter, over a rotation of 180° for 20 min. Image reconstruction was performed with NRecon 1.6.9.8, while 3D visualization utilized DataViewer 1.5.1.2 and CTvox 3.0. Lung CT images were further analyzed using ImageJ software 1.53 (National Institutes of Health, Bethesda, Maryland, USA).

2.7 Measurement of MDA, SOD, GSH and HYP

The levels of malondialdehyde (MDA), superoxide dismutase (SOD), and glutathione (GSH) in lung tissues from PF mice were measured using the corresponding commercial assay kits, following the manufacturers' instructions.

2.8 Detection of ROS

HFL-1 and A549 cells were exposed to DCFH-DA as outlined in the manufacturer's instructions (S0033S, Beyotime, China). The intensity of DCF fluorescence was measured by flow cytometry, using excitation at 485 nm and emission detection at 535 nm to assess cellular fluorescence levels. First, singlet cells were selected based on FSC-A vs. FSC-H to exclude cell aggregates. Live A549 and HFL-1 cells were then gated using the appropriate viability dye. Intracellular ROS levels were measured using DCFH-DA fluorescence. Marker-positive cells were identified based on increased fluorescence intensity compared to the unstained control. All analyses were performed using a BD FACSCanto II flow cytometer and processed with FlowJo software (BD Life Sciences, Ashland, OR, USA).

2.9 Immunofluorescence Staining

Fixed lung tissues, underwent paraffin embedding, were sectioned, and then processed. After applying primary antibodies specific for Nrf2 and p65, the sections were kept at 4 °C overnight to ensure adequate binding. On the following day, secondary antibody incubation was performed for 1 hour at room temperature (25 °C) while protecting the samples from light. Finally, DAPI staining was performed for 10 min, and the sections were mounted. The expression of Nrf2/p65 was analyzed using a Leica SP8 confocal microscope (Leica, Wetzlar, Germany).

2.10 Western Blotting

Proteins extracted from A549 cells or lung tissues were quantified using the BCA method, and equal amounts were subjected to SDS-PAGE, followed by transfer onto nitrocellulose membranes. To prevent nonspecific interactions, membranes were blocked with skim milk, then incubated overnight at 4 °C with primary antibodies that recognize Smad2, Smad3, phosphorylated Smad2/3, Nrf2, HO-1, Keap1, as well as fibrosis markers (α-SMA, COL1A1, fibronectin) and EMT-related proteins (vimentin, E-cadherin, N-cadherin). The next day, secondary antibodies conjugated to horseradish peroxidase were applied for 1 hour at room temperature. Immunoreactive bands were detected using an enhanced ECL system, and images were acquired with the Image Quant 800 instrument.

2.11 Metabolomics Analysis

Blood samples were collected from the abdominal aorta into Eppendorf tubes without anticoagulant and allowed to clot. Serum was separated by centrifugation and preserved at –80 °C. Upon analysis, serum samples were thawed on ice, and 100 μL was combined with 400 μL cold methanol-acetonitrile (1:1, v/v). After incubation at –20 °C for 1 hour to precipitate proteins, samples were centrifuged at 13,000 rpm for 15 minutes at 4 °C. The supernatant was then concentrated and reconstituted for subsequent analyses. QC samples were pooled from equal volumes of each sample.

Chromatography: Chromatographic separation was performed on an ACQUITY UPLC HSS T3 column (100 × 2.1 mm, 1.8 μm) maintained at 40 °C. The mobile phases were 5 mmol/L ammonium acetate with acetic acid (A) and acetonitrile (B). The following gradient was employed: 1% B from 0–1 min, 1–9% B from 1–9 min, 99–1% B from 9–9.1 min, and 1% B from 9.1–12 min. The flow rate was set at 0.35 mL/min, and the sample injection volume was 2 μL.

Mass Spectrometry: ESI was conducted in both positive and negative modes, with the source temperature held

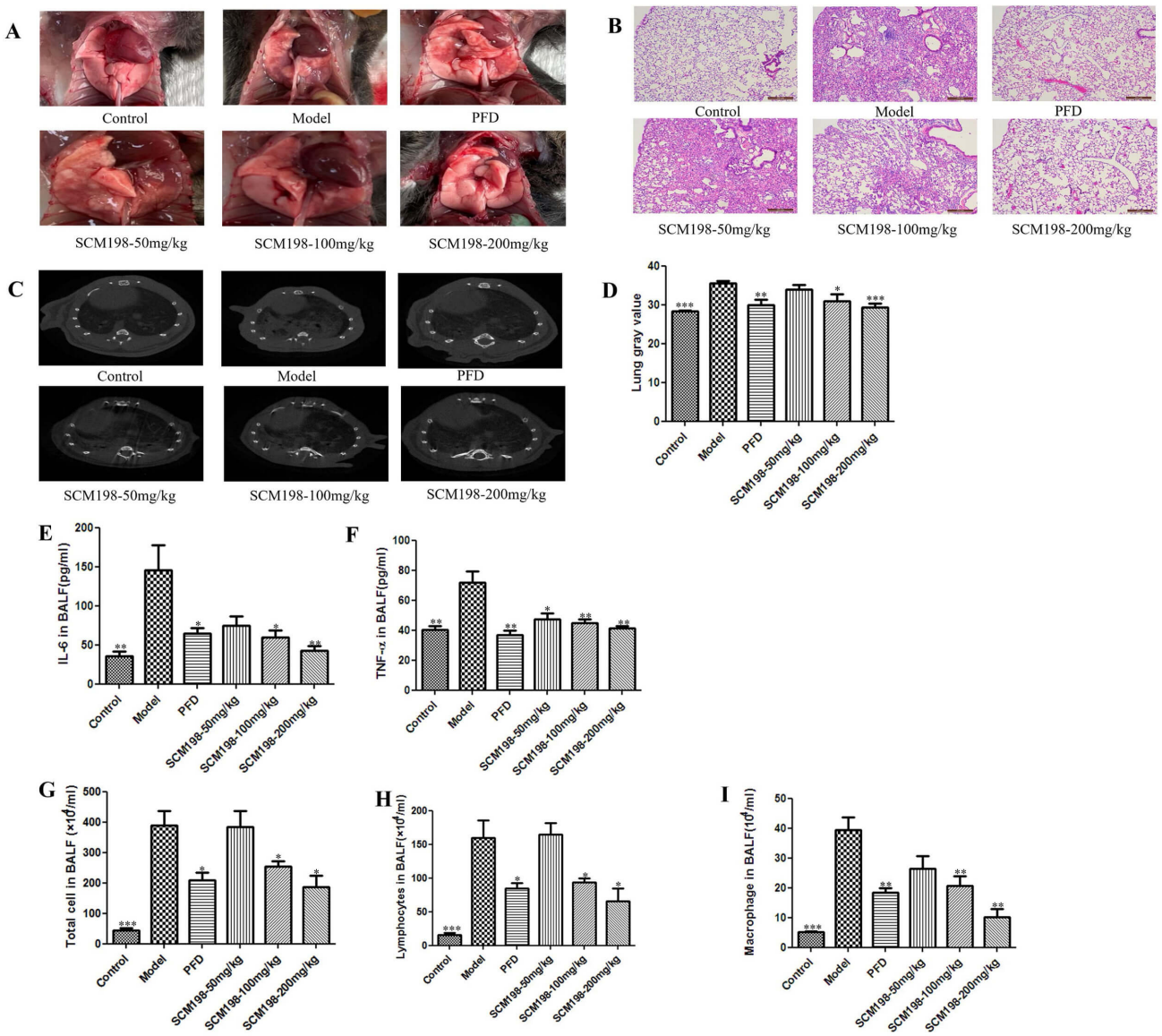

Fig. 1. SCM198 alleviated PF in mice induced by BLM. (A) The anatomy of the lungs was observed. (B) HE-stained lung (magnification ×200, Scale bar = 200 μm). (C,D) Lung CT images of the mice and their quantitative evaluation. (E,F) Concentrations of IL-6 and TNF-α in the BALF. (G) Total cell count in BALF. (H) Lymphocytes count in BALF. (I) Macrophage count in BALF. Results are expressed as mean values ± standard error of the mean (SEM), with a sample size of six per group. Statistical significance relative to the model group was determined as follows: $*p < 0.05$, $**p < 0.01$, $***p < 0.001$. PFD, Pirfenidone; IL-6, Interleukin-6; BALF, Bronchoalveolar Lavage Fluid; TNF-α, Tumor Necrosis Factor-alpha; PF, Pulmonary fibrosis; BLM, Bleomycin; HE, Hematoxylin and Eosin; CT, Computed Tomography.

at 350 °C. Capillary voltages of +3.8 kV and –3.4 kV were applied, while auxiliary and sheath gases were maintained at 15 and 50 arbitrary units, respectively. A full scan & DDA (70–1050 Da, resolution 70,000, AGC 3E6, max IT 100 ms) was performed. The top 5 ions (intensity >100,000) underwent MS/MS (resolution 17,500, max IT 50 ms, 6 s exclusion).

Data were extracted with Progenesis QI 2.4, normalized in MetaboAnalyst 5.0, and analyzed by PLS-DA in SIMCA. Differential metabolites (VIP ≥1, $p < 0.05$, |LogFC| >1) were identified using "fdrtool" in R. HMDB and MetaboAnalyst 5.0 were used for metabolite annotation and pathway analysis.

2.12 Statistical Analysis

All the quantitative data are reported as the mean ± SEM ($\bar{x} \pm s$). Statistical analyses were performed using GraphPad Prism 8.0 (GraphPad Software, LLC, San Diego, CA, USA). One-way Analysis of Variance (ANOVA) followed by Tukey's multiple comparisons was applied for single-factor analyses. For multifactorial data, a two-way ANOVA including interaction effects was used, with Bon-

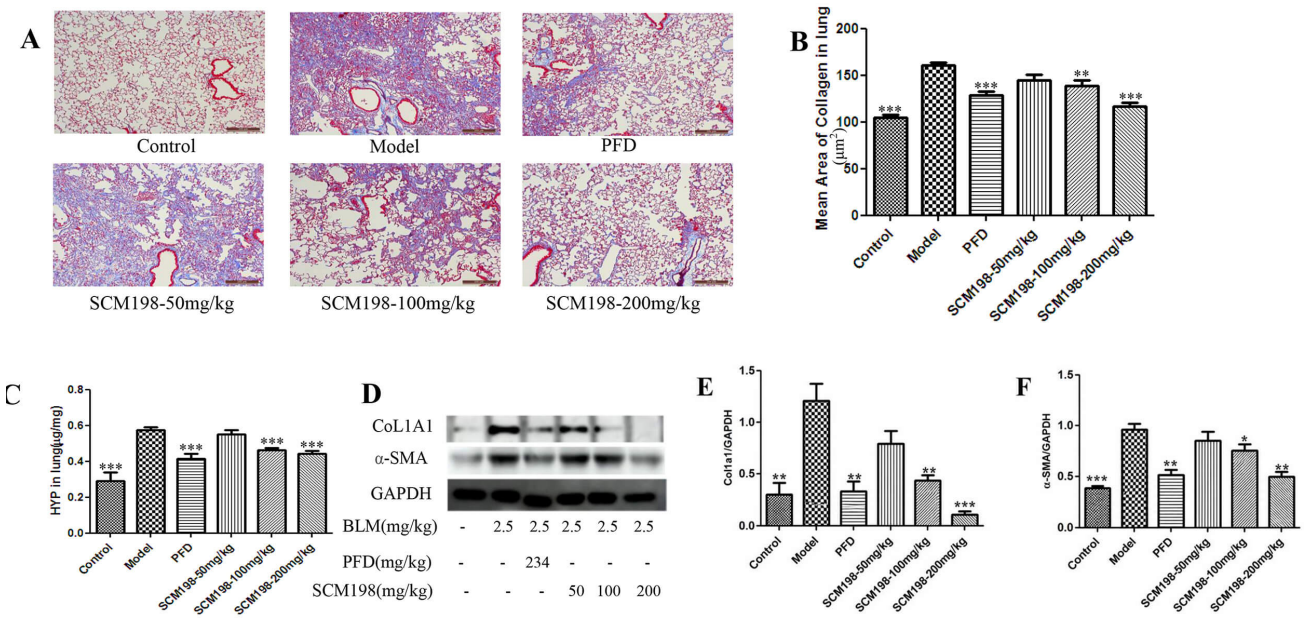

Fig. 2. SCM198 ameliorated lung tissue collagen formation in BLM-induced mice. (A,B) Masson-stained lungs (magnification ×200, Scale bar = 200 μm) and their quantitative evaluation. (C) HYP levels in the lung. (D–F) Quantification and analysis of α-SMA and COL1A1 protein levels in the lungs. The data are presented as the means ± SEMs; n = 6 vs the model group; *$p < 0.05$, **$p < 0.01$, ***$p < 0.001$. HYP, Hydroxyproline; COL1A1, Collagen Type I Alpha 1 Chain; α-SMA, α-smooth muscle actin; GAPDH, Glyceraldehyde-3-Phosphate Dehydrogenase.

ferroni correction for selected comparisons. Results were considered significant at two-sided p values less than 0.05.

3. Results

3.1 SCM198 Ameliorated Pathological and Imaging Changes in BLM-Induced Mice

Visual inspection of the lung tissue in the BLM-treated group revealed congestion and focal necrosis in some areas. Treatment with SCM198 ameliorated these pathological changes (Fig. 1A). H&E staining of lung tissue from PF mice showed structural disruption, increased thickness of the alveolar interstitium, and infiltration of inflammatory cells into the alveoli and interstitial spaces in the model group. SCM198 treatment significantly ameliorated these pathological changes induced by BLM (Fig. 1B). Micro-CT was used to perform *in vivo* lung imaging, and our results demonstrated that SCM198 significantly reduced the abnormalities observed in pulmonary CT images of the BLM-treated mice (Fig. 1C,D). After BLM exposure, AECs were damaged, leading to cell death, which, in turn, led to infiltration of immune cells into the alveoli. We quantified the number of infiltrating inflammatory cells (macrophages and-lymphocytes) and measured the levels of inflammatory cytokines (IL-6 and TNF-α) in the BALF. SCM198 treatment significantly reduced both the number of inflammatory cells and the cytokine levels in the BALF (Fig. 1E–I), indicating that SCM198 effectively mitigates inflammation in the pulmonary system of mice with PF.

3.2 SCM198 Ameliorated Lung Tissue Collagen Formation in BLM-Induced Mice

Collagen content in pulmonary tissue was evaluated using Masson's trichrome staining. Analysis demonstrated a marked elevation of collagen accumulation in the lungs of the model group, whereas SCM198 treatment markedly reduced collagen accumulation (Fig. 2A,B). Hydroxyproline (HYP) levels, a biomarker commonly used to assess the degree of fibrosis, were also significantly decreased by SCM198 in the lungs of mice with PF (Fig. 2C). Furthermore, the expression levels of the PF marker proteins, α-SMA and COL1A1, were assessed. SCM198 significantly reduced the levels of both proteins in the lungs of PF mice (Fig. 2D–F). These findings indicate that SCM198 ameliorates BLM-induced PF.

3.3 SCM198 Inhibited the TGF-β1/Smad2/3 Pathway in BLM-Induced Mice

Protein levels of TGF-β1, as well as total and phosphorylated Smad2 and Smad3, were assessed in lung tissues from BLM-induced pulmonary fibrosis mice. The results indicate that SCM198 treatment led to a significant reduction in TGF-β1 expression and decreased phosphorylation of Smad2 and Smad3 (Fig. 3A–D). Collectively, these data suggest that SCM198 effectively downregulates the TGF-β1/Smad2/3 signaling pathway, thereby mitigating BLM-induced pulmonary fibrosis.

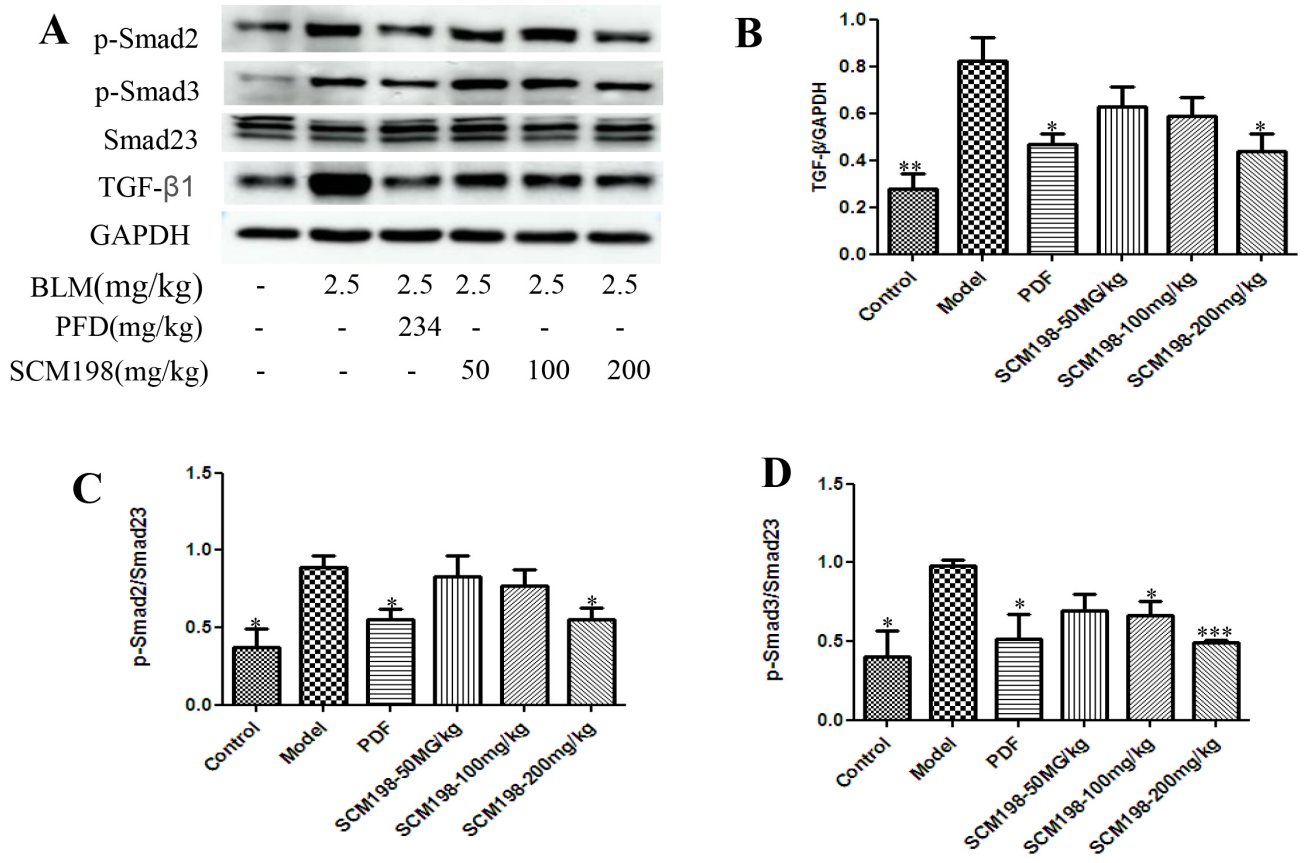

Fig. 3. SCM198 attenuated the TGF-β1/Smad2/3 signaling response in the lungs of BLM-exposed mice. (A) The expression levels of TGF-β1, as well as phosphorylated forms of Smad2 and Smad3. (B) Quantification and analysis of TGF-β1. (C) Quantification and analysis of p-Smad2/Smad2/3. (D) Quantification and analysis of p-Smad3/Smad2/3. The data are presented as the means ± SEMs; n = 6 vs the model group; *$p < 0.05$, **$p < 0.01$, ***$p < 0.001$. TGF-β1, transforming growth factor-beta 1.

3.4 SCM198 Ameliorated Metabolic Disturbances in Metabolite Levels in Mice With BLM-Induced PF

To systematically elucidate the mechanism by which SCM198 ameliorates metabolic disturbances in mice with BLM-induced PF, we conducted a non-targeted metabolomic analysis of serum using the UPLC-Q-TOF/MS platform. This analysis involved characterizing serum metabolites in three groups: a control group, a BLM-induced fibrosis model group, and an SCM198-treated group. The PLS-DA score plot and permutation test (n = 200) (Fig. 4A–D) demonstrated robust model validity and predictive power, clearly distinguishing the metabolic profiles among the three groups. Differential metabolites were detected between the control and model groups, as well as between the model and SCM198 treatment groups, under both ESI+ and ESI− conditions. A total of 30 significantly altered metabolites were detected (10 in ESI+ and 20 in ESI− modes), visualized in a heatmap (Fig. 4E). The categories of these metabolites include lipids and derivatives (8), nucleosides (1), organic heterocyclic compounds (13), amino acids and derivatives (4), organic acids and derivatives (3), and organic nitrogen compounds (1). Pathway enrichment analysis conducted with MetaboAnalyst 5.0 revealed 28 significantly perturbed metabolic pathways (Fig. 4F), primarily related to fatty acid metabolism, phospholipid metabolism, amino acid metabolism, and oxidative phosphorylation. These pathways and their associated metabolites play crucial roles in inflammatory responses, lipid trafficking, OS, and mitochondrial dysfunction. Thus, our findings suggest that the protective effect of SCM198 against BLM-induced PF may be mediated through the modulation of OS-related pathways.

3.5 SCM198 Alleviated BLM-Induced OS in Mice by Activating the NRF2 Signaling Pathway

Our metabolomic analysis indicates that SCM198 might function to ameliorate BLM-induced PF by regulating pathways associated with OS. OS enhances an inflammatory response, leading to damage to and apoptosis in AECs [15,16,17]. SOD, GSH, and MDA are widely recognized indicators of oxidative stress. In this study, their levels were assessed in lung tissues of mice with BLM-induced PF. Our data show that SCM198 significantly reduced MDA levels while increasing GSH and SOD levels in the lung tissues of BLM-induced PF mice (Fig. 5A–C). To evaluate the cellular defense against oxidative stress,

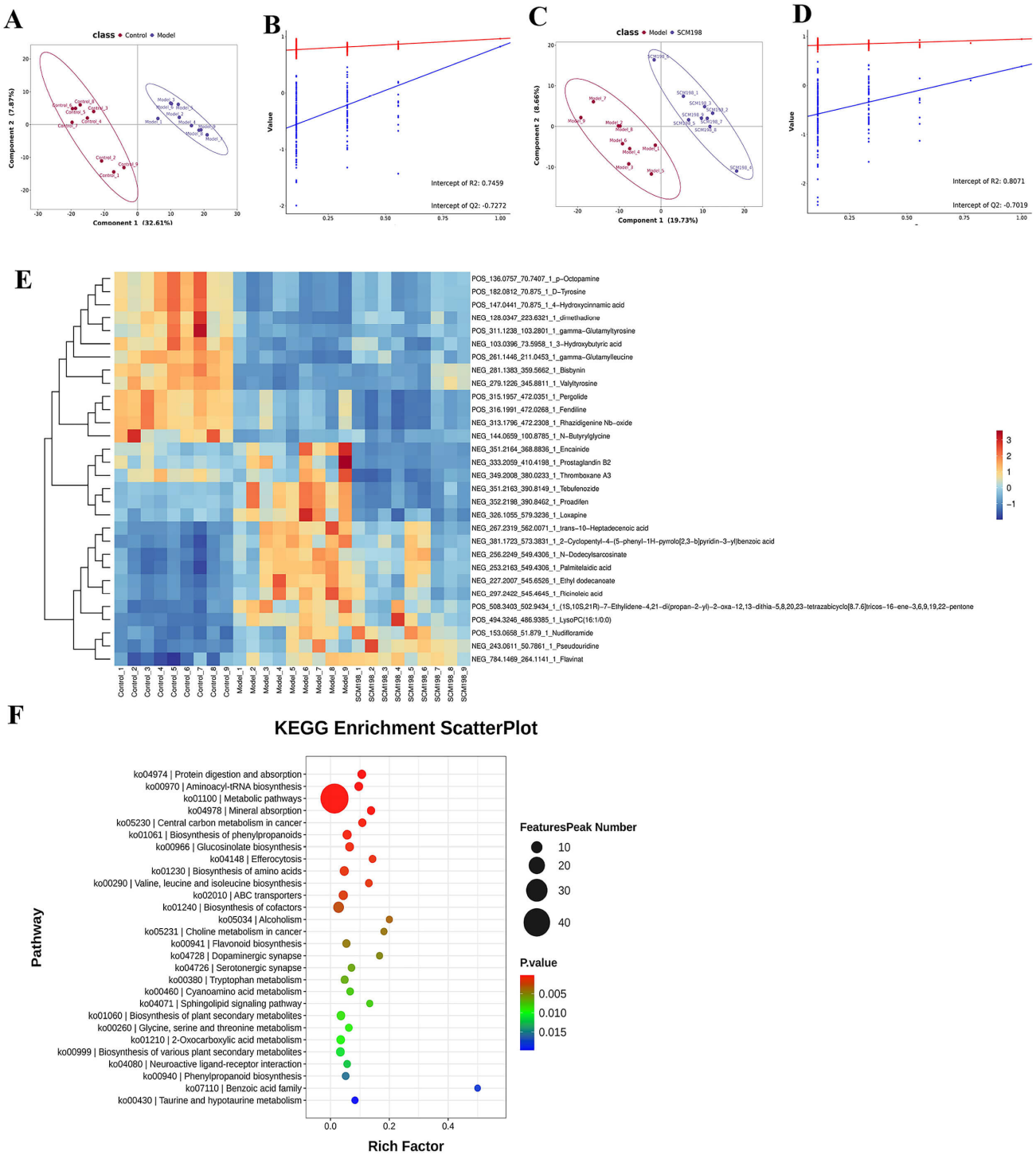

Fig. 4. SCM198 alleviates metabolic disturbances in metabolite levels in mice with BLM-induced PF. (A) Score plots from PLS-DA illustrating differences between control and model groups. (B) Permutation analysis evaluating group separation between control and model groups. (C) PLS-DA score plots indicating distribution between model and SCM198 groups. (D) Permutation testing assessing classification between model and SCM198 groups. (E) Heatmap of differential metabolites. (F) KEGG enrichment factor plot. PLS-DA, Partial Least Squares Discriminant Analysis; KEGG, Kyoto Encyclopedia of Genes and Genomes.

we examined the expression of Keap1, Nrf2, and HO-1 in lung tissue. Following SCM198 administration, Keap1 levels were notably reduced, while HO-1 expression was elevated. Immunohistochemical analysis further confirmed an increase in Nrf2 nuclear translocation in the lungs of mice treated with SCM198 (Fig. 5D–H). These findings indicate that SCM198 effectively inhibits OS in mice with BLM-induced PF by activating the Nrf2 signaling pathway.

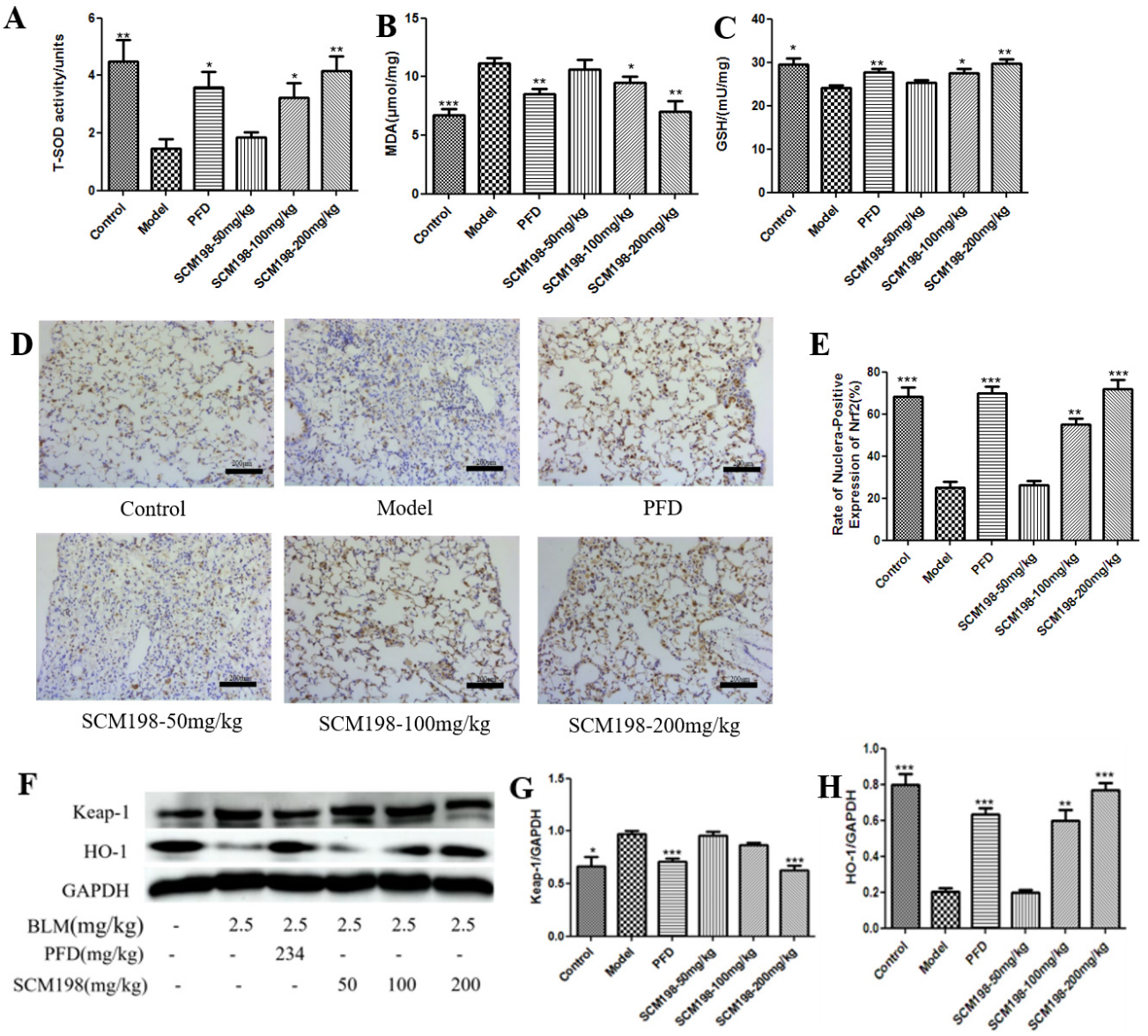

Fig. 5. SCM198 alleviated BLM-induced OS in mice by activating the Nrf2 signalling pathway. (A–C) Concentrations of T-SOD, MDA and GSH in the lungs. (D) Immunohistochemistry analysis of Nrf2 in the lung (magnification ×200, scale bar = 200 μm). (E) Rate of nuclear-positive expression of Nrf2. (F–H) Analysis and quantification of Keap1 and HO-1 in the lung. The data are presented as the means ± SEMs; n = 6 vs the model group; *$p < 0.05$, **$p < 0.01$, ***$p < 0.001$. Keap1, Kelch-like ECH-associated protein 1; HO-1, heme oxygenase-1; OS, oxidative stress; Nrf2, nuclear factor erythroid 2-related factor 2; SOD, Superoxide Dismutase; MDA, Malondialdehyde; GSH, Glutathione.

3.6 SCM198 Inhibited TGF-β1-Induced HFL-1 Cell Activation and EMT in TGF-β1-Induced A549 Cells

The transition of PF into myofibroblasts, and the EMT of AECs, are pivotal pathological processes in the development and progression of PF [18]. TGF-β1 is a well-established inducer of both fibroblast activation and EMT in AECs [19]. In our study, we evaluated the impact of SCM198 on TGF-β1-induced activation of HFL-1 cells and EMT in A549 cells. The findings demonstrated that SCM198 markedly lowered the levels of fibronectin, α-SMA, and COL1A1 in HFL-1 cells (Fig. 6A–D). In addition, treatment with SCM198 in A549 cells led to reduced expression of vimentin and N-cadherin, alongside an up-regulation of E-cadherin (Fig. 6E–H). Collectively, these results indicate that SCM198 suppresses TGF-β1-induced activation in HFL-1 cells and inhibits EMT in A549 cells.

3.7 SCM198 Inhibited the TGF-β1/Smad2/3 Pathway in TGF-β1-Induced HFL-1 Cells and A549 Cells

After TGF-β1 exposure, we assessed Smad2 and Smad3 activation and TGF-β1 protein concentrations in both HFL-1 and A549 cell lines. SCM198 treatment led

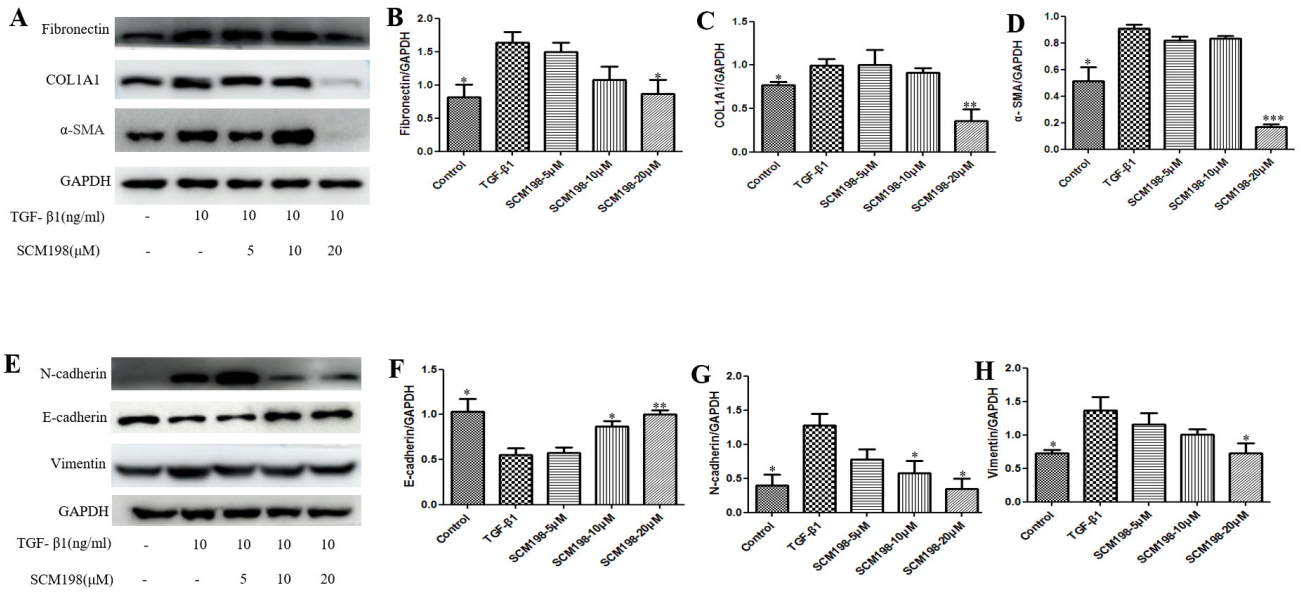

Fig. 6. SCM198 inhibited TGF-β1-induced HFL-1 cell activation and EMT in TGF-β1-induced A549 cells. (A–D) Analysis and quantification of fibronectin, α-SMA, and COL1A1 in HFL-1 cells. (E–H) Analysis and quantification of Vimentin, N-cadherin and E-cadherin in A549 cells. The data are presented as the means ± SEMs; n = 3 vs the model group; *$p < 0.05$, **$p < 0.01$, ***$p < 0.001$. HFL-1, Human Fetal Lung fibroblast-1; EMT, epithelial–mesenchymal transition.

to a clear reduction in the phosphorylation of Smad2 and Smad3 in these cells (Fig. 7A–F). These results suggest that SCM198 markedly suppresses the activation of the TGF-β1/Smad pathway, thus hindering the TGF-β1-induced activation of HFL-1 cells and EMT in TGF-β1-induced A549 cells.

3.8 SCM198 Alleviates OS During TGF-β1-Induced EMT in A549 Cells by Activating the NRF2 Signaling Pathway

Upon exposure to TGF-β1, OS is triggered in both fibroblasts and AECs, subsequently encouraging fibroblast activation and driving EMT in AECs [20]. To assess this, we measured OS levels in TGF-β1-treated A549 and HFL-1 cells. Notably, while ROS levels significantly increased in both cell types following TGF-β1 treatment, SCM198 significantly mitigated ROS levels specifically in A549 cells. This specificity suggests that SCM198 selectively reduces OS during TGF-β1-induced EMT in A549 cells without affecting the OS during the activation of HFL-1 cells (Fig. 8A–D). Further investigation into changes in the Nrf2 signaling pathway revealed that SCM198 treatment significantly decreased Keap1 levels and increased HO-1 levels in TGF-β1-treated A549 cells (Fig. 8E–H). Immunofluorescence data analysis demonstrated enhanced nuclear translocation of Nrf2 in A549 cells (Fig. 8I,J). Thus, these findings illustrate that SCM198 mitigates OS during TGF-β1-induced EMT in A549 cells through the activation of the Nrf2/HO-1 signaling pathway.

4. Discussion

PF is a chronic degenerative interstitial lung disease characterized by an excessive accumulation of ECM in the lungs, which ultimately leads to pulmonary scarring and respiratory failure [21]. SCM198, a synthetic sulfate derivative of leonurine, has been extensively investigated by our group. The findings have demonstrated SCM198's significant anti-inflammatory [22], antioxidative [13], antiapoptotic [23], antimyocardial fibrotic [24], and antiliver fibrotic [25] biological activities, along with a favorable safety profile. Our research has shown that SCM198 markedly improves lung pathology and radiological features in PF mice, reduces collagen accumulation, and decreases the expression of PF marker proteins.

Under conditions of pulmonary injury or inflammatory stimulation, such as induction by TGF-β1, quiescent pulmonary fibroblasts become activated and differentiate into myofibroblasts. These activated fibroblasts synthesize and secrete excessive ECM components at lesion sites and release profibrotic cytokines, including IL-6 and connective tissue growth factor (CTGF). These cytokines amplify the activation of neighboring cells and perpetuate inflammatory responses [26]. Concurrently, AECs undergo EMT in response to injury. This transition is characterized by the downregulation of E-cadherin and the upregulation of N-cadherin and vimentin, enabling AECs to adopt a fibroblast-like phenotype that contributes directly to ECM synthesis and deposition. EMT-transformed cells secrete profibrotic mediators such as TGF-β and PDGF, creating a feedforward loop that further activates fibroblasts and exacerbates fibrotic progression [27,28]. Our findings indicate

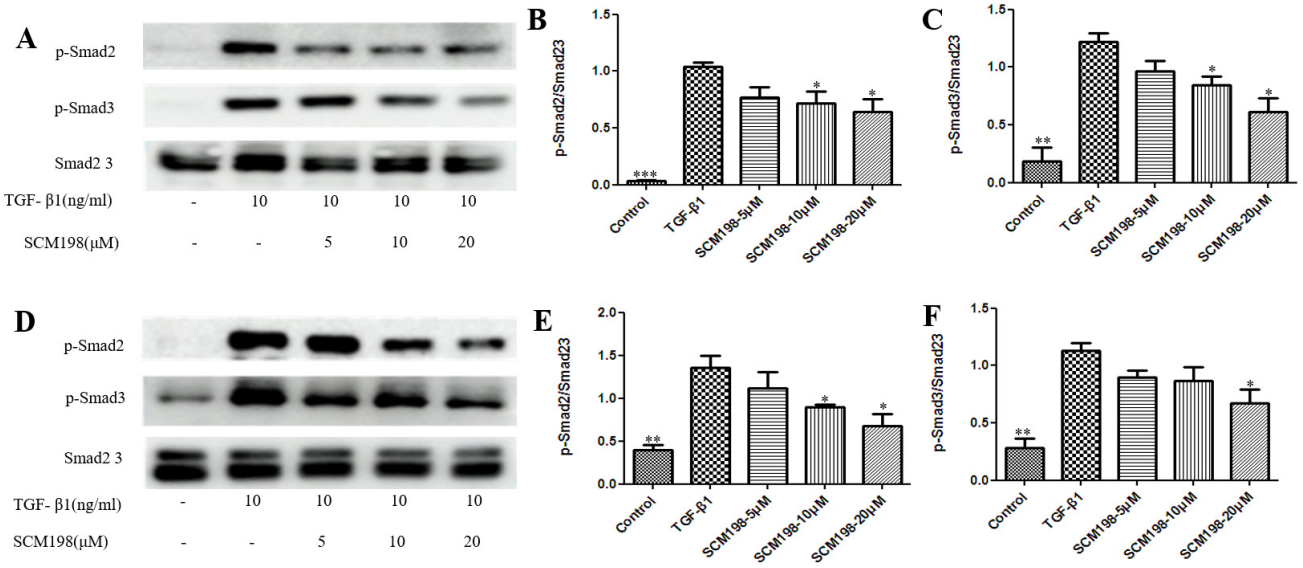

Fig. 7. SCM198 inhibited the TGF-β1/Smad2/3 pathway in TGF-β1-induced HFL-1 cells and A549 cells. (A–C) Phosphorylated Smad2 and Smad3 levels were determined and quantitated in HFL-1 cells. (D–F) Corresponding measurements of p-Smad2 and p-Smad3 were carried out in A549 cells. Data are expressed as mean ± SEM for three independent experiments. Statistical significance compared with the model group is indicated as follows: $*p < 0.05$, $**p < 0.01$, $***p < 0.001$.

that SCM198 significantly inhibits the activation of lung fibroblasts and the EMT in AECs.

TGF-β1/Smad2/3 signaling is integral to pulmonary fibrosis development. Upon receptor engagement, TGF-β1 induces phosphorylation of Smad2 and Smad3, which then join with Smad4 and relocate to the nucleus. There, they interact with distinct DNA regions, consequently adjusting the transcription of genes involved in cell growth, movement, and collagen formation [29]. In models of PF, there is a positive correlation between the hyperactivation of the TGF-β1/Smad2/3 pathway and the severity of fibrotic lesions. Inhibiting the activity of this pathway can effectively mitigate the progression of PF, thereby providing a potential target for the development of novel antifibrotic therapies [30]. Based on our results, SCM198 treatment was associated with reduced activation of pulmonary fibroblasts and EMT of AECs, alongside inhibition of the TGF-β1/Smad2/3 signaling pathway and a corresponding attenuation in ECM deposition. However, further studies involving pathway-specific interventions are needed to establish a direct causal relationship between these observed effects.

Imbalance in fatty acid metabolism, particularly the reduction of polyunsaturated fatty acids, can exacerbate cellular membrane dysfunction and drive pro-fibrotic inflammatory responses by promoting the generation of inflammatory lipid mediators such as prostaglandins. Disruption in phospholipid metabolism compromises the integrity of cell membranes and signaling systems, interferes with repair processes, and aggravates oxidative stress. Reprogramming of amino acid metabolism, including heightened activity in proline and glutamine metabolism, directly supplies synthetic precursors for the abnormal deposition of extracellular matrix components such as collagen, representing a key factor in fibrosis progression. Oxidative phosphorylation, central to cellular energy supply, is impaired in fibrotic conditions-especially in alveolar epithelial cells-leading to an energy deficit and mitochondrial dysfunction. This triggers and amplifies oxidative stress, damages cells, activates fibroblasts, and ultimately promotes fibrosis. In this study, we employed metabolomics to investigate whether SCM198 ameliorates pulmonary fibrosis by inhibiting oxidative stress. These results demonstrate that SCM198 modulates multiple metabolites associated with fatty acid, phospholipid, amino acid metabolism, and oxidative phosphorylation, and are consistent with the hypothesis that SCM198 may exert protective effects against bleomycin-induced pulmonary fibrosis via regulation of oxidative stress-related pathways. However, as functional interference experiments (e.g., pathway-specific inhibitors or gene knockdown) were not performed in this study, a direct causal relationship remains to be further validated. OS promotes the activation of pulmonary fibroblasts and the EMT of AECs, ultimately contributing to ECM formation [31,32]. Our findings demonstrate that SCM198 significantly alleviates OS in various models, including mice with PF and TGF-β-induced A549 cells. However, SCM198 did not mitigate OS during the activation of lung fibroblasts (HFL-1) induced by TGF-β1. This result suggests that the ability of SCM198 to ameliorate PF may involve the inhibition of OS during the EMT of AECs. In this study, *in vivo* results indicate that SCM198 can significantly reduce oxidative stress in lung tissues of mice with pulmonary fibrosis. The discrepancy between the aforementioned *in*

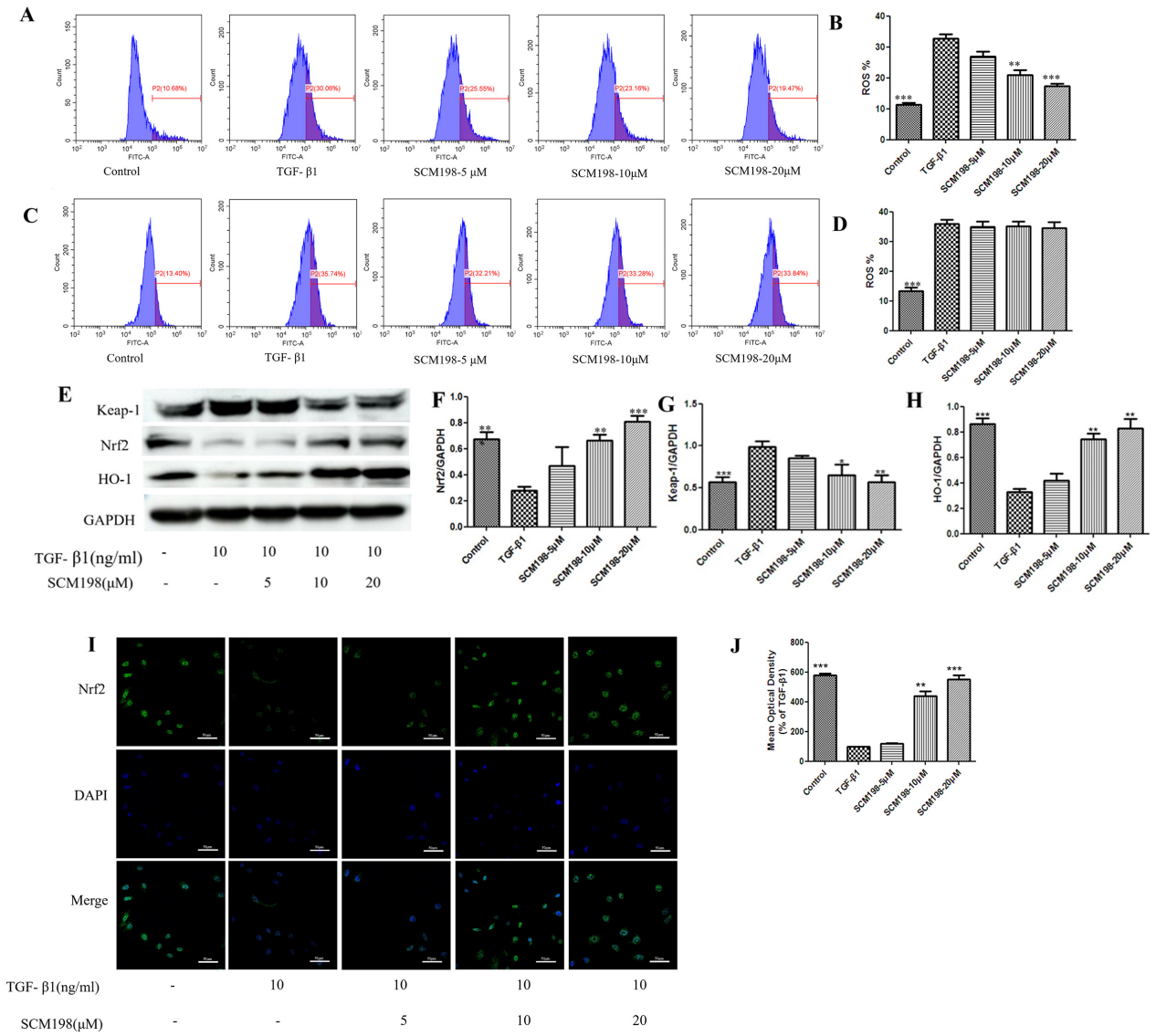

Fig. 8. OS in A549 cells treated with TGF-β1 was ameliorated by SCM198 via activation of the Nrf2 signaling pathway. (A,B) ROS levels were assessed via flow cytometry and quantitatively evaluated in A549 cells. (C,D) ROS levels were assessed via flow cytometry and quantitatively evaluated in HFL-1 cells. (E–H) Analysis and quantification of the Nrf2, Keap1 and HO-1 proteins in A549 cells. (I) Immunofluorescence for Nrf2 in A549 cells. Scale bar: 50 μm. (J) Mean optical density of Nrf2 in A549 cells. Data are presented as the mean ± SEM, n = 3, vs model group, *$p < 0.05$, **$p < 0.01$, ***$p < 0.001$. ROS, reactive oxygen species.

vivo and *in vitro* results may be attributed to the following factors. Research suggests that the Nrf2 pathway in alveolar epithelial cells is relatively sensitive to various stimuli (such as TGF-β1 and cigarette smoke). The endogenous antioxidant defense system in these cells—including the expression and modification status of Nrf2 and its negative regulatory protein Keap1—may render them more responsive to the activation by Leonurine. Simultaneously, in the fibrotic microenvironment induced by TGF-β1, Nrf2 within HFL-1 cells may be degraded more rapidly via the ubiquitin-proteasome pathway. This leads to poor stability, preventing effective accumulation and nuclear translocation even under Leonurine stimulation. In addition, in A549 cells, TGF-β1-induced reactive oxygen species (ROS) mainly originates from mitochondrial dysfunction and activation of NADPH oxidases (such as NOX4). The Nrf2 pathway activated by Leonurine can effectively suppress ROS generation from these sources. However, in HFL-1 cells, the mechanisms of ROS production during fibroblast-to-myofibroblast transition may be more complex and resilient. Beyond NOX family members, it may involve alterations in other enzymatic systems (e.g., xanthine oxidase) or metabolic pathways. The Leonurine-Nrf2 axis might not adequately target the primary sources of ROS in HFL-1 cells. Therefore, this study has certain limitations. More comprehensive experiments—such as employing different lung fibroblast lines and inhibiting the Nrf2 signaling pathway—are needed to further elucidate

the underlying mechanisms. Most researchers concur that the Nrf2/HO-1 signaling pathway plays a crucial role in protecting cells from OS-induced damage [33,34]. Nrf2, a widely expressed transcriptional activator, is highly expressed in the lungs during detoxification responses. Numerous studies have demonstrated that activation of the Nrf2/HO-1 signaling pathway can effectively eliminate excess ROS [35]. Our results show that SCM198 treatment is associated with activation of the Nrf2 signaling pathway and reduced oxidative stress during the EMT of AECs, which may contribute to the attenuation of PF. However, it should be noted that these findings are primarily correlative, and further mechanistic studies are required to confirm these observations and establish a direct causal relationship.

In summary, our experimental data indicated that SCM198 ameliorates PF induced by BLM. Additionally, we have demonstrated that the mechanism by which SCM198 ameliorates PF may involve downregulating the TGF-β1/Smad pathway and activating Nrf2-mediated antioxidant activity during EMT.

5. Limitations

This study is subject to some limitations, which are mainly reflected in the following three aspects. This study is subject to several limitations. First, although peripheral blood metabolomic profiling in our mouse model of pulmonary fibrosis suggested that SCM198 may ameliorate fibrosis by modulating oxidative stress, we did not perform targeted validation of specific metabolites. Second, while we assessed classical EMT markers (E-cadherin, N-cadherin, vimentin) in A549 cells, we did not evaluate key mesenchymal transcription factors such as Snail, Slug, or ZEB1, which are important for confirming the EMT process. In HFL-1 cells, we only analyzed major fibroblast activation markers (α-SMA, COL1A1, and fibronectin), but did not include proliferation markers (e.g., Ki67), nor did we conduct additional functional assays, such as wound healing, Transwell migration, or collagen gel contraction. These shortcomings may affect the comprehensiveness of our mechanistic characterization. Third, although our results strongly suggest that SCM198 attenuates pulmonary fibrosis by downregulating the TGF-β1/Smad2/3 pathway and activating Nrf2-mediated antioxidant defenses during EMT, our evidence is primarily correlative. We did not perform further gain- or loss-of-function experiments, such as siRNA-mediated knockdown of Nrf2 or Smad2/3, or pharmacological inhibition of TGF-β receptor (e.g., SB431542), which would have provided more direct mechanistic insights. Thus, further studies using genetic or pharmacological interventions are required to establish a definite causal relationship between SCM198 and the TGF-β1/Smad and Nrf2 pathways in pulmonary fibrosis. Despite these limitations, our findings provide a valuable foundation for future in-depth mechanistic investigations.

6. Conclusions

In summary, our experimental data suggest that SCM198 attenuates BLM-induced pulmonary fibrosis. The underlying mechanisms may involve downregulation of the TGF-β1/Smad pathway and activation of Nrf2-mediated antioxidant activity during EMT, but these findings remain correlative and require further direct validation in future studies through genetic or pharmacological interventions.

Abbreviations

BALF, bronchoalveolar lavage fluid; BLM, Bleomycin; EMT, epithelial–mesenchymal transition; FBS, Fetal Bovine Serum; HO-1, Heme Oxygenase 1; HYP, Hydroxyproline; Keap1, Kelch-like ECH-associated protein 1; MDA, Malondialdehyde; Nrf2, Nuclear factor erythroid 2-related factor 2; OS, oxidative stress; PF, Pulmonary fibrosis; PS, Penicillin–Streptomycin; PFD, Pirfenidone; ROS, reactive oxygen species; SOD, Superoxide Dismutase; TGF-β1, Transforming Growth Factor Beta 1; GSH, Glutathione; AECs, alveolar epithelial cells.

Availability of Data and Materials

The data presented in this study are available upon request from the corresponding author.

Author Contributions

Conceptualization, JL, YZ; methodology, JL, HW, RW, KC and JL; formal analysis, KC and JL; writing-original draft preparation, JL; project administration, YZ; funding acquisition, YZ. All the authors have read and agreed to the final version of the manuscript. All authors contributed to editorial changes in the manuscript. All authors have participated sufficiently in the work and agreed to be accountable for all aspects of the work.

Ethics Approval and Consent to Participate

The Ethics Committee of Macau University of Science and Technology approved this study. Approval number (MUST-SSTIC-20250507001). The study was carried out in accordance with the ARRIVE guidelines and the Chinese national standard GB/T 35892-2018.

Acknowledgment

The authors wish to thank the State Key Laboratory of Mechanism and Quality of Chinese Medicine (Macau University of Science and Technology) and the Laboratory of Drug Discovery from Natural Resources and Industrialization for their support.

Funding

Funded by The Science and Technology Development Fund, Macau SAR (File no. 0001/2024/RDP).

Conflicts of Interest

The authors declare that they have no conflicts of interest. The funders had no role in the design of the study; in the collection, analyses, or interpretation of data; in the writing of the manuscript; or in the decision to publish the results.

Supplementary Material

Supplementary material associated with this article can be found, in the online version, at https://doi.org/10.31083/Pharmazie52723.

References

[1] Collard HR, Ryerson CJ, Corte TJ, Jenkins G, Kondoh Y, Lederer DJ, et al. Acute Exacerbation of Idiopathic Pulmonary Fibrosis. An International Working Group Report. American Journal of Respiratory and Critical Care Medicine. 2016; 194: 265–275. https://doi.org/10.1164/rccm.201604-0801CI

[2] Martinez FJ, Collard HR, Pardo A, Raghu G, Richeldi L, Selman M, et al. Idiopathic pulmonary fibrosis. Nature Reviews. Disease Primers. 2017; 3: 17074. https://doi.org/10.1038/nrdp.2017.74

[3] George PM, Wells AU, Jenkins RG. Pulmonary fibrosis and COVID-19: the potential role for antifibrotic therapy. The Lancet. Respiratory Medicine. 2020; 8: 807–815. https://doi.org/10.1016/S2213-2600(20)30225-3

[4] Podolanczuk AJ, Thomson CC, Remy-Jardin M, Richeldi L, Martinez FJ, Kolb M, et al. Idiopathic pulmonary fibrosis: state of the art for 2023. The European Respiratory Journal. 2023; 61: 2200957. https://doi.org/10.1183/13993003.00957-2022

[5] Lv Q, Wang J, Xu C, Huang X, Ruan Z, Dai Y. Pirfenidone alleviates pulmonary fibrosis in vitro and in vivo through regulating Wnt/GSK-3β/β-catenin and TGF-β1/Smad2/3 signaling pathways. Molecular Medicine (Cambridge, Mass.). 2020; 26: 49. https://doi.org/10.1186/s10020-020-00173-3

[6] Pan L, Cheng Y, Yang W, Wu X, Zhu H, Hu M, et al. Nintedanib Ameliorates Bleomycin-Induced Pulmonary Fibrosis, Inflammation, Apoptosis, and Oxidative Stress by Modulating PI3K/Akt/mTOR Pathway in Mice. Inflammation. 2023; 46: 1531–1542. https://doi.org/10.1007/s10753-023-01825-2

[7] Zhao M, Wang M, Chen X, Gao Y, Chen Q, Wang L, et al. Targeting progranulin alleviated silica particles-induced pulmonary inflammation and fibrosis via decreasing Il-6 and Tgf-β1/Smad. Journal of Hazardous Materials. 2024; 465: 133199. https://doi.org/10.1016/j.jhazmat.2023.133199

[8] Chen JY, Yang YJ, Meng XY, Lin RH, Tian XY, Zhang Y, et al. Oxysophoridine inhibits oxidative stress and inflammation in hepatic fibrosis via regulating Nrf2 and NF-κB pathways. Phytomedicine: International Journal of Phytotherapy and Phytopharmacology. 2024; 132: 155585. https://doi.org/10.1016/j.phymed.2024.155585

[9] Liu Y, Wang S, Jin G, Gao K, Wang S, Zhang X, et al. Network pharmacology-based study on the mechanism of ShenKang injection in diabetic kidney disease through Keap1/Nrf2/Ho-1 signaling pathway. Phytomedicine: International Journal of Phytotherapy and Phytopharmacology. 2023; 118: 154915. https://doi.org/10.1016/j.phymed.2023.154915

[10] Liu C, Guo W, Maerz S, Gu X, Zhu Y. 3,5-Dimethoxy-4-(3-(2-carbonyl-ethyldisulfanyl)-propionyl)-benzoic acid 4-guanidino-butyl ester: a novel twin drug that prevents primary cardiac myocytes from hypoxia-induced apoptosis. European Journal of Pharmacology. 2013; 700: 118–126. https://doi.org/10.1016/j.ejphar.2012.11.028

[11] Liu XH, Pan LL, Deng HY, Xiong QH, Wu D, Huang GY, et al. Leonurine (SCM-198) attenuates myocardial fibrotic response via inhibition of NADPH oxidase 4. Free Radical Biology & Medicine. 2013; 54: 93–104. https://doi.org/10.1016/j.freeradbiomed.2012.10.555

[12] Meng S, Song Z, Tang Z, Yang X, Xiao Y, Guo H, et al. Surface-decorated nanoliposomal leonurine targets activated fibroblast-like synoviocytes for efficient rheumatoid arthritis therapy. Biomaterials Science. 2023; 11: 7099–7113. https://doi.org/10.1039/d3bm00911d

[13] Zhao B, Peng Q, Wang D, Zhou R, Wang R, Zhu Y, et al. Leonurine Protects Bone Mesenchymal Stem Cells from Oxidative Stress by Activating Mitophagy through PI3K/Akt/mTOR Pathway. Cells. 2022; 11: 1724. https://doi.org/10.3390/cells11111724

[14] Zhang L, Tong X, Huang J, Wu M, Zhang S, Wang D, et al. Fisetin Alleviated Bleomycin-Induced Pulmonary Fibrosis Partly by Rescuing Alveolar Epithelial Cells From Senescence. Frontiers in Pharmacology. 2020; 11: 553690. https://doi.org/10.3389/fphar.2020.553690

[15] Dinesh Babu V, Suresh Kumar A, Sudhandiran G. Diosgenin inhibits TGF-β1/Smad signaling and regulates epithelial mesenchymal transition in experimental pulmonary fibrosis. Drug and Chemical Toxicology. 2022; 45: 1264–1275. https://doi.org/10.1080/01480545.2020.1814803

[16] Peng L, Wen L, Shi QF, Gao F, Huang B, Meng J, et al. Scutellarin ameliorates pulmonary fibrosis through inhibiting NF-κB/NLRP3-mediated epithelial-mesenchymal transition and inflammation. Cell Death & Disease. 2020; 11: 978. https://doi.org/10.1038/s41419-020-03178-2

[17] Zhao J, Ma X, Li S, Liu C, Liu Y, Tan J, et al. Berberine hydrochloride ameliorates PM2.5-induced pulmonary fibrosis in mice through inhibiting oxidative stress and inflammatory. Chemico-biological Interactions. 2023; 386: 110731. https://doi.org/10.1016/j.cbi.2023.110731

[18] Andugulapati SB, Gourishetti K, Tirunavalli SK, Shaikh TB, Sistla R. Biochanin-A ameliorates pulmonary fibrosis by suppressing the TGF-β mediated EMT, myofibroblasts differentiation and collagen deposition in in vitro and in vivo systems. Phytomedicine: International Journal of Phytotherapy and Phytopharmacology. 2020; 78: 153298. https://doi.org/10.1016/j.phymed.2020.153298

[19] Liu TT, Sun HF, Tang MZ, Shen HR, Shen Z, Han YX, et al. Bicyclol attenuates pulmonary fibrosis with silicosis via both canonical and non-canonical TGF-β1 signaling pathways. Journal of Translational Medicine. 2024; 22: 682. https://doi.org/10.1186/s12967-024-05399-x

[20] Qian W, Cai X, Qian Q, Zhang W, Wang D. Astragaloside IV modulates TGF-β1-dependent epithelial-mesenchymal transition in bleomycin-induced pulmonary fibrosis. Journal of Cellular and Molecular Medicine. 2018; 22: 4354–4365. https://doi.org/10.1111/jcmm.13725

[21] Koudstaal T, Funke-Chambour M, Kreuter M, Molyneaux PL, Wijsenbeek MS. Pulmonary fibrosis: from pathogenesis to clinical decision-making. Trends in Molecular Medicine. 2023; 29: 1076–1087. https://doi.org/10.1016/j.molmed.2023.08.010

[22] Liu XH, Pan LL, Yang HB, Gong QH, Zhu YZ. Leonurine attenuates lipopolysaccharide-induced inflammatory responses in human endothelial cells: involvement of reactive oxygen species and NF-κB pathways. European Journal of Pharmacology. 2012; 680: 108–114. https://doi.org/10.1016/j.ejphar.2012.01.012

[23] Xin H, Liu XH, Zhu YZ. Herba leonurine attenuates doxorubicin-induced apoptosis in H9c2 cardiac muscle cells. European Journal of Pharmacology. 2009; 612: 75–79. https://doi.org/10.1016/j.ejphar.2009.03.067

[24] Li Z, Chen K, Zhu YZ. Leonurine inhibits cardiomyocyte pyroptosis to attenuate cardiac fibrosis via the TGF-β/Smad2 sig-

nalling pathway. PLoS ONE. 2022; 17: e0275258. https://doi.org/10.1371/journal.pone.0275258

[25] Wang P, Bai J, Ye M, Huang Z, Chen J, Sun L, et al. Leonurine Attenuates CCl_4-Induced Hepatic Fibrosis in Mice via the Hippo-YAP Pathway. Drug Design, Development and Therapy. 2025; 19: 6553–6571. https://doi.org/10.2147/DDDT.S518793

[26] Tang Q, Xing C, Li M, Jia Q, Bo C, Zhang Z. Pirfenidone ameliorates pulmonary inflammation and fibrosis in a rat silicosis model by inhibiting macrophage polarization and JAK2/STAT3 signaling pathways. Ecotoxicology and Environmental Safety. 2022; 244: 114066. https://doi.org/10.1016/j.ecoenv.2022.114066

[27] Liu W, Han X, Li Q, Sun L, Wang J. Iguratimod ameliorates bleomycin-induced pulmonary fibrosis by inhibiting the EMT process and NLRP3 inflammasome activation. Biomedicine & Pharmacotherapy. 2022; 153: 113460. https://doi.org/10.1016/j.biopha.2022.113460

[28] Qiu C, Zhao Z, Xu C, Yuan R, Ha Y, Tu Q, et al. Nebulized milk exosomes loaded with siTGF-β1 ameliorate pulmonary fibrosis by inhibiting EMT pathway and enhancing collagen permeability. Journal of Nanobiotechnology. 2024; 22: 434. https://doi.org/10.1186/s12951-024-02721-z

[29] Li Y, Qin W, Liang Q, Zeng J, Yang Q, Chen Y, et al. Bufei huoxue capsule alleviates bleomycin-induced pulmonary fibrosis in mice via TGF-β1/Smad2/3 signaling. Journal of Ethnopharmacology. 2023; 316: 116733. https://doi.org/10.1016/j.jep.2023.116733

[30] Shao W, Zhang J, Yao Z, Zhao P, Li B, Tang W, et al. Cannabidiol suppresses silica-induced pulmonary inflammation and fibrosis through regulating NLRP3/TGF-β1/Smad2/3 pathway. International Immunopharmacology. 2024; 142: 113088. https://doi.org/10.1016/j.intimp.2024.113088

[31] Yang H, Wang L, Yang M, Hu J, Zhang E, Peng L. Oridonin attenuates LPS-induced early pulmonary fibrosis by regulating impaired autophagy, oxidative stress, inflammation and EMT. European Journal of Pharmacology. 2022; 923: 174931. https://doi.org/10.1016/j.ejphar.2022.174931

[32] Ding Y, Wang L, Liu B, Ren G, Okubo R, Yu J, et al. Bryodulcosigenin attenuates bleomycin-induced pulmonary fibrosis via inhibiting AMPK-mediated mesenchymal epithelial transition and oxidative stress. Phytotherapy Research: PTR. 2022; 36: 3911–3923. https://doi.org/10.1002/ptr.7535

[33] Mohamed AE, Mahmoud AM, Mohamed WR, Mohamed T. Femtosecond laser attenuates oxidative stress, inflammation, and liver fibrosis in rats: Possible role of PPARγ and Nrf2/HO-1 signaling. Life Sciences. 2022; 307: 120877. https://doi.org/10.1016/j.lfs.2022.120877

[34] Chien LH, Deng JS, Jiang WP, Chou YN, Lin JG, Huang GJ. Evaluation of lung protection of Sanghuangporus sanghuang through TLR4/NF-κB/MAPK, keap1/Nrf2/HO-1, CaMKK/AMPK/Sirt1, and TGF-β/SMAD3 signaling pathways mediating apoptosis and autophagy. Biomedicine & Pharmacotherapy. 2023; 165: 115080. https://doi.org/10.1016/j.biopha.2023.115080

[35] Patel D, Yadav P, Singh SK, Tanwar SS, Sehrawat A, Khurana A, et al. Betaine alleviates doxorubicin-induced nephrotoxicity by preventing oxidative insults, inflammation, and fibrosis through the modulation of Nrf2/HO-1/NLRP3 and TGF-β expression. Journal of Biochemical and Molecular Toxicology. 2024; 38: e23559. https://doi.org/10.1002/jbt.23559